

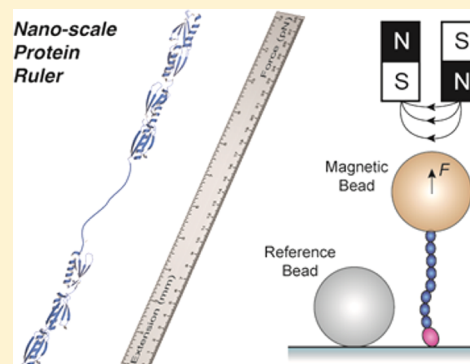
A HaloTag Anchored Ruler for Week-Long Studies of Protein Dynamics

Ionel Popa,^{*,†} Jaime Andrés Rivas-Pardo, Edward C. Eckels, Daniel J. Echelman, Carmen L. Badilla, Jessica Valle-Orero, and Julio M. Fernández^{*}

Department of Biological Sciences, Columbia University, 1212 Amsterdam Avenue, New York, New York 10027, United States

S Supporting Information

ABSTRACT: Under physiological conditions, protein oxidation and misfolding occur with very low probability and on long times scales. Single-molecule techniques provide the ability to distinguish between properly folded and damaged proteins that are otherwise masked in ensemble measurements. However, at physiological conditions these rare events occur with a time constant of several hours, inaccessible to current single-molecule approaches. Here we present a magnetic-tweezers-based technique that allows, for the first time, the study of folding of single proteins during week-long experiments. This technique combines HaloTag anchoring, sub-micrometer positioning of magnets, and an active correction of the focal drift. Using this technique and protein L as a molecular template, we generate a magnet law by correlating the distance between the magnet and the measuring paramagnetic bead with unfolding/folding steps. We demonstrate that, using this magnet law, we can accurately measure the dynamics of proteins over a wide range of forces, with minimal dispersion from bead to bead. We also show that the force calibration remains invariant over week-long experiments applied to the same single proteins. The approach demonstrated in this Article opens new, exciting ways to examine proteins on the “human” time scale and establishes magnetic tweezers as a valuable technique to study low-probability events that occur during protein folding under force.



INTRODUCTION

Proteins inside the cell are constantly being recycled in order to maintain an adequate functionality of the entire proteome.¹ Usually, proteins can reversibly unfold and then return to the functioning native state. However, certain environmental conditions such as redox stress or signaling can modulate the lifetime of proteins² and subsequently alter their capability to carry out their function. It is thought that these conditions trap the protein in an irreversible unfolded or misfolded state, which is associated with cytotoxicity and numerous diseases. Single misfolding events are rare and occur on long time scales (days to weeks), making them difficult to observe in cellular or biochemical assays.³ Force spectroscopy is a technique that can distinguish between folded and unfolded states in a single protein domain, but advances in stability and attachment chemistry are needed to probe single molecules on the time scales associated with misfolding.

Force-clamp spectroscopy allows for the measurement of protein dynamics in response to well-defined force protocols. This technique, implemented with an atomic force microscope, has been used to measure the rates of protein folding and chemical reactions, such as thiol–disulfide exchange and disulfide isomerization.^{2d,4} Force-clamp AFM makes use of an active feedback with a time constant that can approach 1 ms.⁵ The biggest limitation of this approach is the mechanical drift of the AFM instrument. Drift limits the duration of a single-

molecule experiment to a few minutes and decreases accuracy at low forces. By contrast, magnetic tweezers is inherently stable and provides force-clamp conditions without feedback; therefore, it is an ideal instrument to study protein dynamics under force-clamp conditions in the low-force regime. Recent advances in tethering chemistry applied to force spectroscopy now allow for the study of covalently anchored proteins without the risk of detachment.⁶ The low-drift and high force resolution of magnetic tweezers combined with HaloTag anchored proteins constitutes an ideal approach to study protein dynamics at low forces. A limiting factor in the use of magnetic tweezers to study short proteins at low force is due to the difficulty in estimating precisely the applied force.⁷ Brownian fluctuations have been used to measure the force applied to short proteins tethered to paramagnetic beads.^{6c,7} However, its direct use is questionable in the study of protein folding/unfolding reactions. Under mechanical force, proteins show folding/unfolding transitions as step-changes in the measured end-to-end length.⁸ These transitions dominate the motion of the paramagnetic bead at low forces, severely limiting the use of spectral analysis to measure the pulling force (Figure 1). Furthermore, owing to the proteins' short length (20–300 nm), the measuring paramagnetic bead is forced to operate

Received: May 26, 2016

Published: July 13, 2016

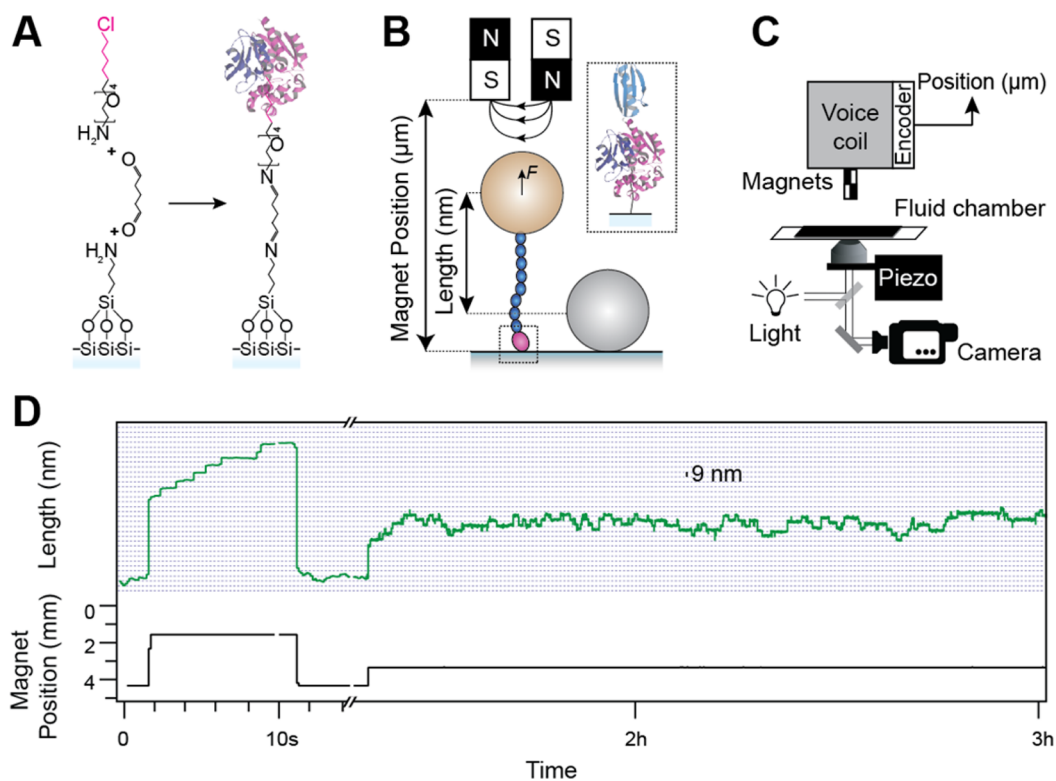


Figure 1. Voice-coil magnetic tweezers with HaloTag attachment measures the folding dynamics of polyproteins under force. (A) HaloTag surface chemistry. An amine-terminated silanized surface is cross-linked to an amine-terminated chloroalkane ligand using glutaraldehyde. We study a fusion protein consisting of a HaloTag followed by eight repeats of protein L and terminated by an AviTag (HaloTag-(protein L)₈-AviTag). The HaloTag is reacted with the chloroalkane ligand on the glass surface, forming a covalent anchor for the construct. (B) The AviTag at the other end of the construct is reacted with a streptavidin-coated paramagnetic bead (gold). The pulling force is adjusted by positioning a pair of permanent magnets at a fixed distance (Magnet Position) above the glass surface. The length of the protein under force is measured with respect to a fiducial nonmagnetic bead affixed to the glass surface (gray). (C) Schematics of the voice-coil tweezers setup. The applied force on the paramagnetic bead is precisely controlled by attaching a pair of permanent magnets to a voice-coil actuator with a 1 cm range and a maximal velocity of ~ 0.7 m/s. An embedded encoder reports on the magnet position with 150 nm resolution. This arrangement allows for the application of fast, arbitrary and repeatable force pulses to the protein. The remainder is a standard magnetic tweezers setup including a piezo-mounted objective, an inverted microscope and a high-speed CCD camera. (D) A long-term experiment using the voice-coil tweezers. The top trace shows the protein length, and the bottom trace reports the magnet position. The protein is first fully unfolded at MP = 1.4 mm (high force), refolded at MP = 4.3 mm (low force), and finally allowed to equilibrate over 3 h at MP = 3.3 mm. The folding/unfolding dynamics of the protein precludes the use of fluctuation analysis to measure the applied force.

near a surface with its associated effects on viscosity and anisotropy. Here we use protein L folding dynamics^{7,9} to demonstrate a novel approach for calibrating the pulling force applied by a magnetic tweezers to short recombinant proteins. Once the calibration is established, it can be applied to different proteins and over extended periods of time with little variance.

We demonstrate that the force-dependent step sizes of the folding/unfolding transitions⁷ can be used to derive a magnet law that precisely calculates the force applied to a protein, solely based on the distance between the magnets and the paramagnetic bead. The use of a magnet law demands precise and stable positioning of the magnets, in order to trust that the applied force is not drifting over time and can be reproduced from one experiment to the next. Furthermore, it is also essential that the magnets can be positioned fast and with high accuracy, and that the paramagnetic beads show a narrow dispersity in their magnetic properties. We demonstrate the remarkable stability of our magnetic tweezers instrument over hours-long recordings of protein L dynamics at low forces. We further expand the measuring time of these experiments to up to 2 weeks and measure the dynamics under force of the same protein with minimal drift.

METHODS

1. Magnetic Tweezers Setup. Our custom-made setups are built on top of an inverted microscope (Olympus IX-71/Zeiss Axiovert S100) using 63 \times oil-immersion objective (Zeiss/Olympus), mounted on a nanofocusing piezo actuator (P-725; Physik Instrumente) and a 1.6 \times optivar lens. The fluid chamber was illuminated using a collimated cold white LED (Thor Labs). Images were acquired using a CCD Pike F-032b camera (Allied Vision Technologies) operating at 280 Hz or a Zyla 5.5 sCMOS camera (Andor), operating at up to 1030 Hz. Paramagnetic Dynabeads M-270 beads with a diameter of 2.8 μ m (Invitrogen) were exposed to force using a pair of permanent neodymium grade N52 magnets (D33, K&J Magnetics), approaching the fluid cell from the top (Figure 1). The position of the magnets was controlled with a linear voice-coil (LFA-2010; Equipment Solutions), which is capable of moving 10 mm with ~ 0.7 m/s speed and 150 nm position resolution. For long-term recordings, an *xy*-stage moving with ~ 100 nm resolution (M-686, Physik Instrumente) was incorporated in order to address identical bead coordinates over separate days. The data acquisition and control of the voice-coil and piezo actuator were done using a multifunction DAQ card (NI USB-6341, National Instruments).

2. Image Processing. Image processing was done using custom-written software in Igor Pro (Wavemetrics), which is described in detail in the SI. In brief, the *z*-position displacement of a bead was

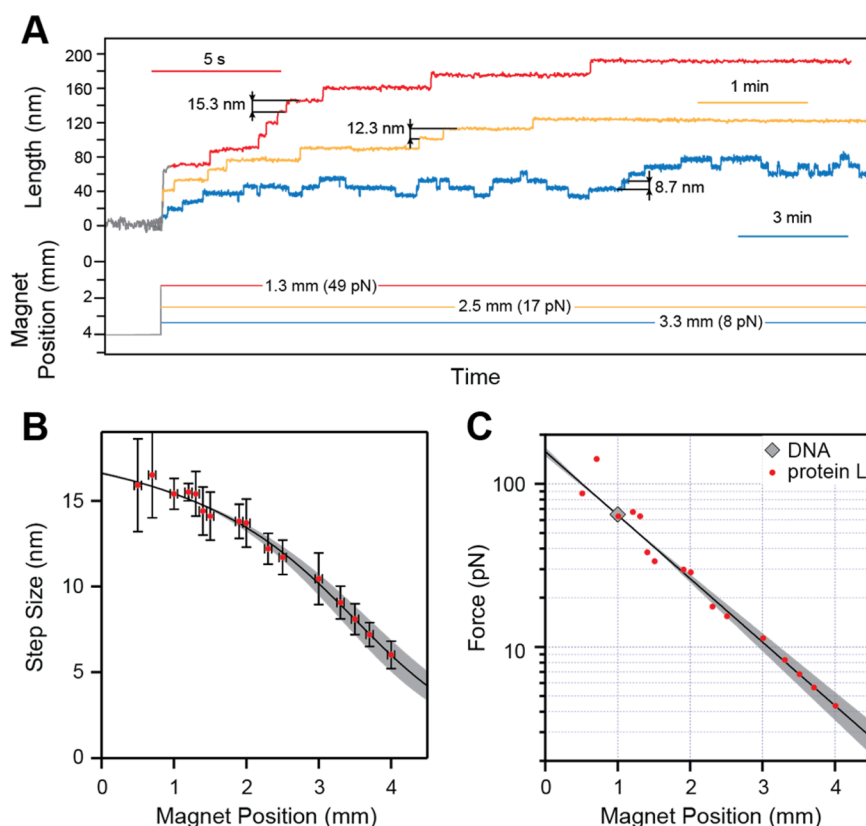


Figure 2. Determination of the magnet law. (A) Unfolding traces of our eight-domain protein L construct (top) measured at three different magnet positions (bottom). Both the unfolding rate and the step sizes scale with the applied force. (B) Average step size of unfolding and folding as a function of magnet position (red dots; error bars indicate standard deviations, data obtained from over 50 different experiments). The solid line is a fit of eq 4 to the data. The shaded area shows the 95% confidence contour. (C) Magnet law derived from B (solid line; eq 5). The red dots correspond to the force calculated from the WLC model for the step sizes measured at different magnet positions (B). The diamond marks the force and magnet position for the B–S transition.

determined in a three-step process: (1) Fourier transform (FFT) of the bead was acquired; (2) the radial profile was computed from the FFT with a pixel-addressing algorithm (FKA algorithm, see SI software); (3) radial profiles were correlated to a z-stack library of the bead acquired prior to the experiment (see SI; Figure S1). The z-position displacement was calculated for the paramagnetic bead tethered to protein, and for a local fixed reference bead used to correct for instrumental vibration and focal drift. With this procedure, frame rates of ~ 1 kHz are achievable.

3. Fluid Chamber Preparation. The single-molecule magnetic tweezers measurements were done in fluid chambers made of two sandwiched glass coverslips (Ted Pella) separated by strips of parafilm. The bottom surfaces were successively cleaned by sonication for 20 min in 1% Hellmanex (Hellma), acetone and ethanol (both from Sigma-Aldrich). After drying with air, the bottom surfaces were exposed to air plasma for 20 min, and silanized by immersion for 20 min in a solution of (3-aminopropyl)-trimethoxysilane (Sigma-Aldrich) 0.1% v/v, in ethanol. After washing unreacted silane with ethanol, the surfaces were cured at 100 °C for >1 h. The top glass surfaces were cleaned by sonication in 1% Hellmanex for 20 min and washed with ethanol. To eliminate reflection of incident light from the magnets, the top glass was coated with either a nonreflective black tape or a 60 nm layer of Ni/Cr and 40 nm of gold (Good Fellow, using an Edwards Auto 306 Vacuum Coating System). For long-term magnetic tweezers experiments, glass coverslips with an imprinted 50 μm^2 grid array (Ibidi) were used to allow for repeated addressing of individual beads over multiple days (Figure S2). These coverslips were cleaned similarly, with the exception of air plasma and silane curing at 100 °C which was replaced with a 24 h vacuum step.

After assembly, the chambers were incubated for 1 h with a solution of glutaraldehyde 1% v/v (Sigma-Aldrich) diluted in PBS buffer, pH

7.2. The fluid chamber was then filled with 0.025% w/v amine-terminated nonmagnetic polystyrene beads with diameter of 2.89 μm (Spherotech), diluted in PBS. After 10 min, the beads that did not adsorb were washed with 100 μL PBS buffer. The chambers were then reacted for >4 h with a solution of 10 $\mu\text{g}/\text{mL}$ HaloTag amine (O4) ligand (Promega), diluted in the same PBS buffer. Finally, the fluid chambers were blocked for 12 h with TRIS blocking buffer: 20 mM Tris-HCl pH 7.4, 150 mM NaCl, 2 mM MgCl_2 and 1% w/v sulfhydryl blocked-BSA (Lee Biosolutions).

4. Protein Expression, Purification, and Modification.

Polyprotein constructs were engineered using a combination of *Bam*HI, *Bgl*III, and *Kpn*I restriction sites, as described previously.¹⁰ The protein constructs had eight repeats of protein L (B1 domain from *Peptostreptococcus magnus*),¹¹ I27, or 9-domain ubiquitin, flanked by an N-terminal HaloTag enzyme (Promega) and a C-terminal AviTag for biotinylation. Proteins cross-linked with DNA had eight repeated domains of protein L or I27^{C47/63A} engineered between a HaloTag at the N-terminus and a cysteine residue at the C-terminus. For purification purposes, a His₆-tag was also present before the AviTag or the cysteine residue. The multidomain proteins were expressed and purified as follows. BLR (DE3) or ERL competent cells containing the engineered pFN18A expression vector (Promega) were grown at 37 °C until $\text{OD}_{600\text{ nm}} \approx 0.6$ –0.8. The protein overexpression was induced with 1 mM Isopropyl β -D-1-thiogalactopyranoside (IPTG, Sigma) overnight at 25 °C. Cells were resuspended in 50 mM sodium phosphate buffer pH 7.0, 300 mM NaCl, 10% glycerol and 1 mM Dithiothreitol (DTT, Sigma), and disrupted by French press. The proteins were purified from the lysate following a two-step procedure: with a Ni–NTA affinity purification resin (GE), followed by size exclusion chromatography using a Superdex–200 HR column (GE) in 10 mM HEPES buffer pH 7.2, 150 mM NaCl, 10% glycerol and 1 mM

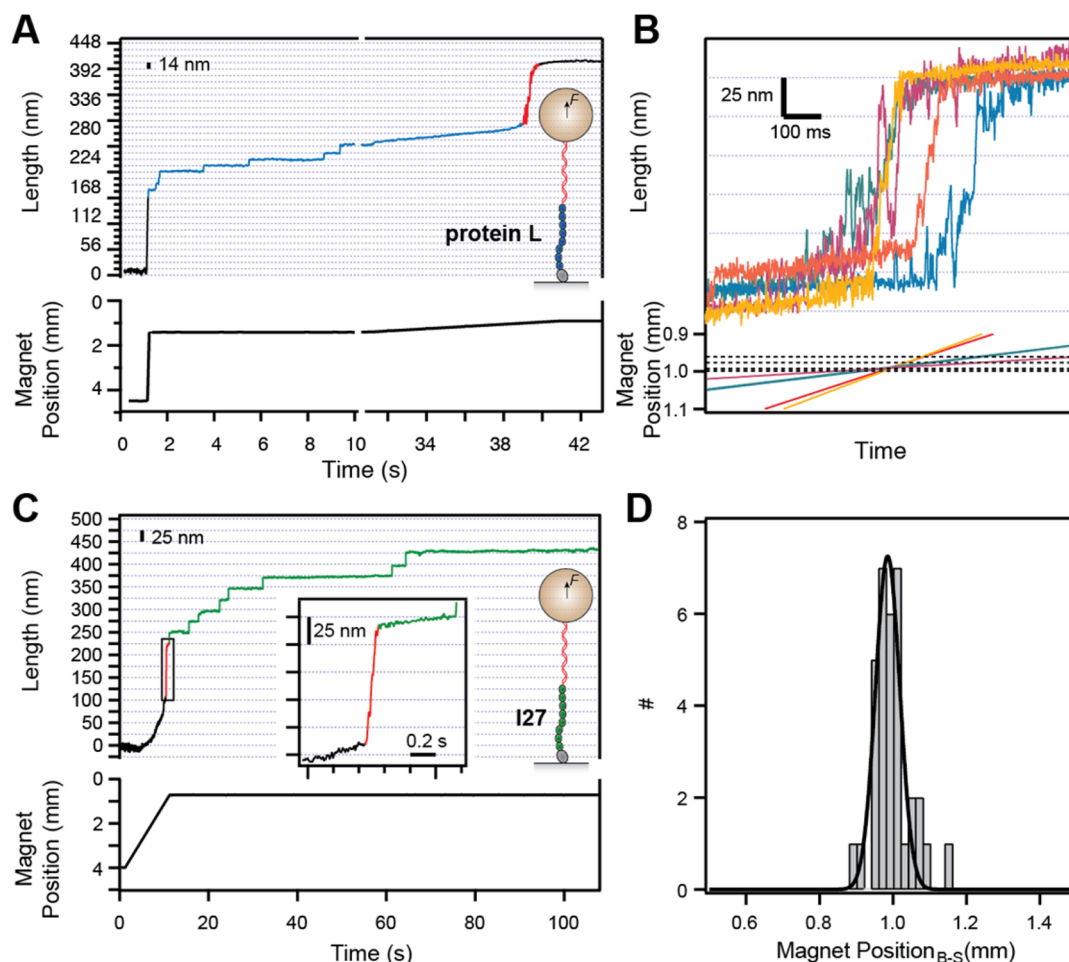


Figure 3. Fiduciary marker for the magnet law, using the B–S overstretching transition. (A) A protein–DNA construct composed of HaloTag–(protein L)₈–cys protein cross-linked to a 605 bp DNA segment is tethered between a glass slide and a paramagnetic bead. The protein–DNA construct is first exposed to a constant force (MP = 1.4 mm), where protein L unfolds in steps of ~14 nm (blue), followed by a ramp-increase in force (from MP = 1.4 to 0.9 mm). (B) The B–S transition is observed at MP ≈ 0.99, marking the 65 pN point. (C) Similar experiment using the more stable titin I27 protein (HaloTag–I27₈–cys). In this case the I27 domains unfold at forces higher than the B–S transition. (D) Histogram of magnet position values where the B–S transition is measured in both I27 and protein L constructs. The line is a Gaussian fit with MP = 0.99 ± 0.05 mm ($n = 34$ traces, 10 different beads).

EDTA. The purified multidomain proteins were pooled and concentrated to 50–100 μ M before biotinylation. Biotinylation was performed in 50 mM Bicine buffer pH 8.3, 10 mM magnesium acetate, 10 mM ATP, 100 μ M biotin and 2.5 μ g biotin ligase BirA enzyme (Avidity), at 30 °C, for 4 h. The biotinylation of the multidomain protein was confirmed through Western blotting, using conjugated streptavidin horseradish peroxidase (GE).

For the synthesis of DNA–protein constructs, a DNA segment from λ -phage DNA (Thermo Scientific) was amplified with amine and biotin primers (IDT) using a standard PCR mix (New England Biolabs), which resulted in a 605 bp DNA linker. The amine end of DNA was reacted with sulfo-SMCC (Thermo Scientific) for 1 h in a solution of Borax buffer pH 8.5 at room temperature. The sulfo-SMCC excess was removed using a PCR cleanup kit (NucleoSpin) and eluting with water. The reaction with the cysteine-terminated protein was done overnight in HEPES buffer, pH 7.2. The cross-linking reaction was confirmed using SDS polyacrylamide gels, stained with ethidium bromide (Figure S3).

5. Single-Molecule Measurements. The protein was freshly diluted in TRIS blocking buffer (20 mM Tris-HCl pH 7.4, 150 mM NaCl, 2 mM MgCl₂ and 1% w/v sulfhydryl-blocked BSA) to ~0.01 μ M and left to adsorb on the surface of the fluid chamber for 10 min. Chambers were then washed with TRIS blocking buffer, and streptavidin coated paramagnetic beads (Dynabeads M-270, Invitrogen) were added to bind with the protein for ~1 min, before

approaching the magnets to a low-force position (4 mm). The protein experiments were performed in TRIS blocking buffer, while the protein–DNA experiments were performed in TRIS blocking buffer lacking MgCl₂. Experiments began after a z-stack library of both a protein-tethered paramagnetic bead and a fixed reference bead were acquired, and real-time z-position displacements were calculated using our image processing method (see SI, Figure S1).

The step sizes describing the unfolding and refolding of individual protein domains were measured from individual traces (Figure S4). For the low-force conditions, a boxcar filter (typically 50 points) was applied beforehand. Length histograms were obtained from the data corresponding to each step, and the absolute position was measured using a Gaussian fit.¹² The size of each step was then obtained from the position of two consecutive histograms (Figure S4). The unfolding rates were calculated from the average traces assuming a single exponential unfolding kinetics.

RESULTS AND DISCUSSION

Our experimental approach is based on magnetic tweezers, a technique capable of applying mechanical force to single molecules via paramagnetic beads (Figure 1). This approach is now extended by the use of HaloTag-based covalent attachment chemistry, which allows for the exposure of single proteins to a mechanical force for extended periods of time

without detachment.^{6b} In magnetic tweezers, the applied force is often calculated using a calibration curve that measures force as a function of the distance between the magnet and the paramagnetic bead tethered to the molecule under study.¹³ The applied force directly depends on the size and magnetic properties of the beads and the geometry and strength of the magnets. It was recently shown that a magnet law can accurately estimate the force on micrometer-long DNA molecules.¹⁴ Here we extend this approach by demonstrating a new method for obtaining the magnet law that applies to short proteins. We use the folding step sizes of protein L as a nanoscale ruler for the change in force with magnet position. When exposed to a constant force, protein L domains undergo unfolding transitions as step-size increases in the measured end-to-end length (Figure 2A). Protein L unfolds within several seconds in steps of 15.3 nm at magnet position 1.3 mm and within 2 min in steps of 12.3 nm at magnet position 2.5 mm. At magnet position 3.3 mm protein L reaches a steady state where unfolding and refolding steps of 8.7 nm are observed over an extended period of time (Figure 2A). The force scaling of the unfolding step sizes is also apparent in the length of the fully unfolded protein (eight domains in all cases; Figure 2A). Folding steps also scale with the pulling force and, for a given force, have the same size as the unfolding steps (Figure S4). Figure 2B recapitulates these data, showing how the step sizes vary with magnet position.

Already the first studies on the unfolding of titin molecules under force showed that the stepwise increases in contour length of an unfolding protein are well described by simple polymer physics models.¹⁵ Both the worm-like chain (WLC) and freely jointed chain (FJC) models produce equivalent results and are used interchangeably through the force spectroscopy literature.^{8b,15c} Similarly, the data shown in Figure 2B can be accurately fit by the WLC model using the protein L parameters of persistence length $p = 0.58$ nm and contour length of $\Delta L_c = 18.6$ nm,⁷ assuming an exponential magnet law given by

$$F = a e^{-bMP} \quad (1)$$

We then combine this magnet law with the WLC model to give

$$MP(x) = -\frac{1}{b} \ln \left\{ \frac{1}{a} \frac{k_B T}{p} \left[\frac{1}{4} \left(1 - \frac{x}{\Delta L_c} \right)^{-2} - \frac{1}{4} + \frac{x}{\Delta L_c} \right] \right\} \quad (2)$$

where MP is the magnet position, x is the observed step size, and a and b are fitting parameters. Fitting the data of Figure 2B using eq 2 gives values of $a = 177 \pm 17$ pN and $b = 1.07 \pm 0.05$ mm⁻¹. In order to refine the accuracy of this magnet law, we take advantage of a well-known force standard—the B–S overstretching transition of DNA molecules. This transition takes place at a well-defined force of 65 pN, independent of the loading rate.¹⁶ By including this fiduciary measurement, the magnet law becomes

$$F(MP) = F_{B-S} e^{b(MP_{B-S} - MP)} \quad (3)$$

where F_{B-S} is the force at which the B–S transition is observed in DNA (65 pN), and MP_{B-S} is the magnet position where the B–S transition is observed in our magnetic tweezers instrument. We measure MP_{B-S} with the experimental approach shown in Figure 3. We engineered a polyprotein containing a

HaloTag followed by eight domains of protein L and a terminal cysteine anchored to a 605 bp DNA linker (see Methods). When we apply a high force to this construct ($MP = 1.4$ mm; Figure 3A), we observe eight ~ 14 nm unfolding steps. As the magnet position is decreased linearly (increasing force), we then observe the overstretching transition as a sharp extension of 127 ± 28 nm (Figure 3A,B), at a magnet position of $MP_{B-S} = 0.99 \pm 0.05$ mm ($n = 34$; Figure 3D). A similar construct composed of eight repeats of the more mechanically stable I27 protein and the same DNA segment¹⁷ first shows the overstretching transition at the same 0.99 mm magnet position, followed by eight ~ 25 nm steps, characteristic of the unfolding of I27 (Figure 3C).

We now combine eq 3 with the WLC model to give

$$MP(x) = MP_{B-S} - \frac{1}{b} \ln \left\{ \frac{1}{F_{B-S}} \frac{k_B T}{p} \left[\frac{1}{4} \left(1 - \frac{x}{\Delta L_c} \right)^{-2} - \frac{1}{4} + \frac{x}{\Delta L_c} \right] \right\} \quad (4)$$

This equation now gives a closed form for $MP(x)$, with b as the only fitting parameter. We fit eq 4 to the data of Figure 2B using the Levenberg–Marquardt least orthogonal distance method with a confidence level of 95% (solid line, Figure 2B). From the fit we obtain $b = 0.90 \pm 0.03$ mm⁻¹, for $F_{B-S} = 65$ pN. The fit was weighted with the standard deviation of the measured extension steps (Figure 2B) and a standard deviation for the magnet position of 0.05 mm, as measured from the DNA–protein experiments (Figure 3D). The shading in Figure 2B marks the upper and lower confidence contours of the fit.

We now have all the parameters needed to establish our magnet law as defined by eq 3:

$$F(MP) = 65 e^{0.9(0.99 - MP)} \quad (5)$$

We verify the goodness of this magnet law in Figure 2C. We plot the predicted force for each step size calculated using the WLC, as a function of the MP where the steps were measured (red dots; Figure 2C). We also mark the position of the overstretching B–S transition in DNA (open square; Figure 2C). The data shown in this figure are compared with the magnet law given by eq 5 (solid line with shading at 95% confidence; Figure 2C). In Figure S5 we explore the parameter sensitivity of our magnet law. We impose deviations of 5 pN for F_{B-S} ,¹⁴ of 0.1 nm for p , and of 0.3 nm for ΔL_c .¹⁸ The impact of these parameter variations on the magnet law is within the 95% confidence level.

In addition to protein L, we have also measured unfolding and folding step sizes for ubiquitin and I27 polyproteins (Figure S6). The increase in contour length upon unfolding (ΔL_c) is protein specific as it depends on the number of amino acids entrapped in the folded structure: $\Delta L_c = 18.6$ nm for protein L, $\Delta L_c = 24.5$ nm for ubiquitin,¹⁹ and $\Delta L_c = 28.4$ nm for I27.¹⁸ We readily reproduce the force dependency of the steps sizes for these proteins by using eq 4 with the corresponding values of ΔL_c (Figure S6).

The magnet law defined by eq 5 is valid as long as the instrument remains stable during the measurements, implying that the relationship between magnet position and force is time and molecule independent. To correct for focal drift over such long time scales, we actively adjust the position of the objective using a piezo actuator such that the position of a nonmagnetic

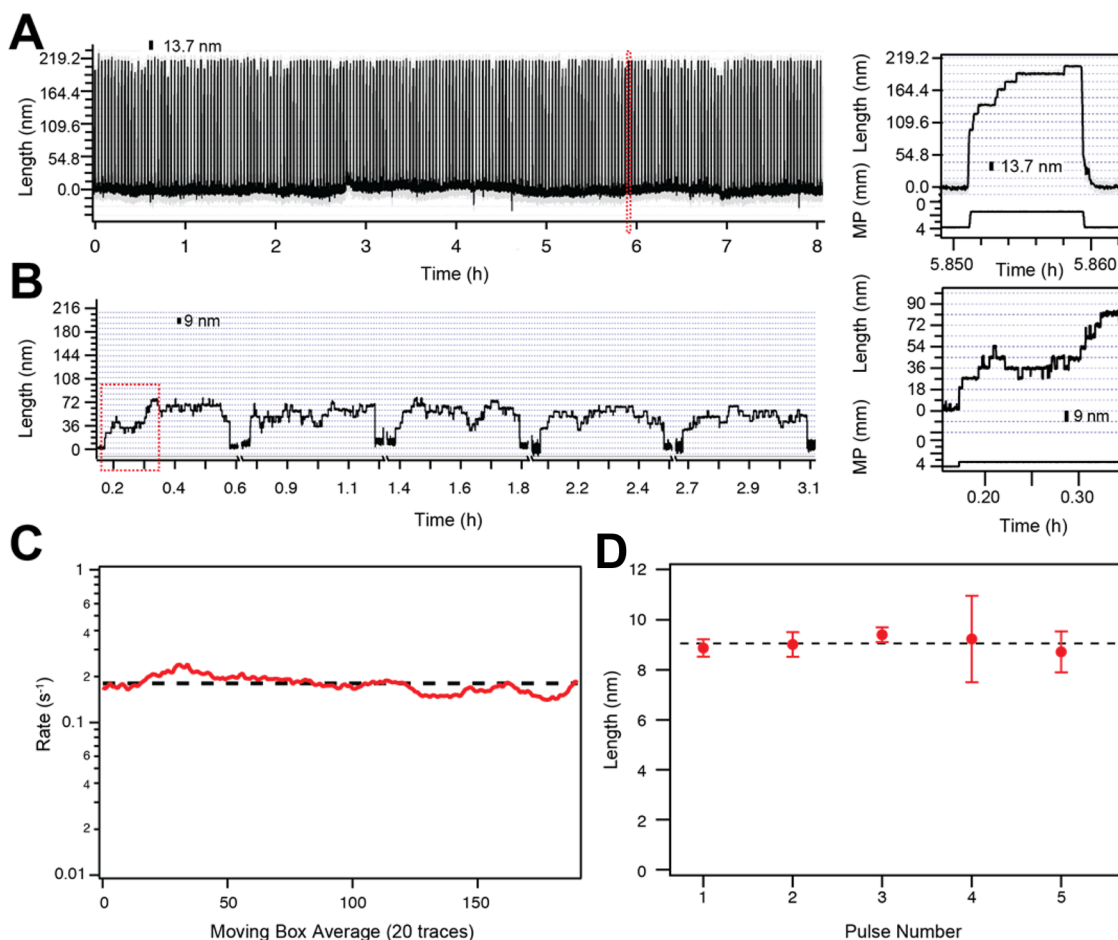


Figure 4. Stability of the voice-coil tweezers over hours-long recordings of HaloTag anchored proteins. (A) Unfolding/folding cycles of an anchored HaloTag-(protein L)₈-AviTag protein obtained by alternating the force from 45 pN to 4.3 pN (MP = 1.4–4 mm). The inset on the right magnifies a single unfolding trace from the 8-h-long recording (left, red box). (B) Similar recording as in (A), but pulsing to a lower force of 8 pN (MP = 3.3 mm). (C) Unfolding rate obtained from a moving box average of 20 consecutive traces taken from the trace in (A) gives a mean rate of 0.20 ± 0.02 s⁻¹ at 45 pN. (D) Average step size per pulse (B; 9.0 ± 0.4 nm).

reference bead is maintained at a constant value (see also [Methods](#) and [SI](#)). Due to the exponential dependency of force with magnet position, we expect that errors will become more significant at high forces. As a proxy for errors in the high-force regime, we measure the unfolding rates of protein L over extended periods of time, which in this case is a better indicator for drift in force than the step size (which saturates at high forces, see discussion below) ([Figure 4A,C](#)). A single protein L construct was continuously exposed to unfolding-refolding cycles for >8 h ([Figure 4A](#)). These cycles consisted of unfolding the protein with 30-s pulses to 45 pN (MP = 1.4 mm), after which the protein was allowed to refold at 4.3 pN (MP = 4 mm). A moving average of 20 unfolding traces was fit with a single exponential to measure the unfolding rate over the 8-h-long experiment. [Figure 4C](#) shows the measured unfolding rates (mean rate of 0.20 ± 0.02 s⁻¹) over the full length of the trace. The mean unfolding rate of the first 100 boxes is not significantly different compared with the last 100 boxes (0.21 ± 0.02 s⁻¹ and 0.19 ± 0.02 s⁻¹, respectively). The observed rate variations, if arising solely from instrumental error, correspond to changes in force of ± 2 pN (SD rates).

Another measure for the stability of our magnetic tweezers instrument is the distribution of unfolding and refolding step sizes, which were used as the basis for determining the magnet law ([Figure 2B](#)). Following the shape of the WLC model of

polymer elasticity, the step sizes are relatively invariant at the high end of the force law. However, at forces below 20 pN, the step sizes change rapidly with force, hence providing a good measure of stability in this range. [Figure 4B](#) shows several 25-min-long unfolding pulses at 8 pN (MP = 3.3 mm) showing numerous unfolding and refolding steps as the protein equilibrates. From these data we measured the average step size in each pulse ([Figure 4D](#)), showing that these measurements are remarkably stable. The mean value of the step sizes at 8 pN is 9.0 ± 0.4 nm ([Figure 4D](#)), which is very close to the value predicted by the WLC model (8.9 nm). At this force, the domains are kept unfolded for longer times than at 45 pN, and after 3 h some domains failed to refold. Therefore, we have not included data longer than 3 h at this force.

The experiment shown in [Figure 5](#) further extends the observations shown in [Figure 4](#) to a single protein L construct experiment lasting 14 days. In this case, a single protein L construct is probed (afternoons) by unfolding at 45 pN for 45 s (MP = 1.4 mm; [Figure 5A](#)). For such long experiments, we exposed the molecules to high force only several times a day, so as to minimize the dissociation of the biotin–streptavidin and detachment of the paramagnetic bead. In between force pulses, the molecule was held at 4.3 pN (MP = 4.0 mm). Importantly, rates of unfolding were comparable between measuring days ([Figure 5B](#)). Moreover, the mean of the unfolding step sizes

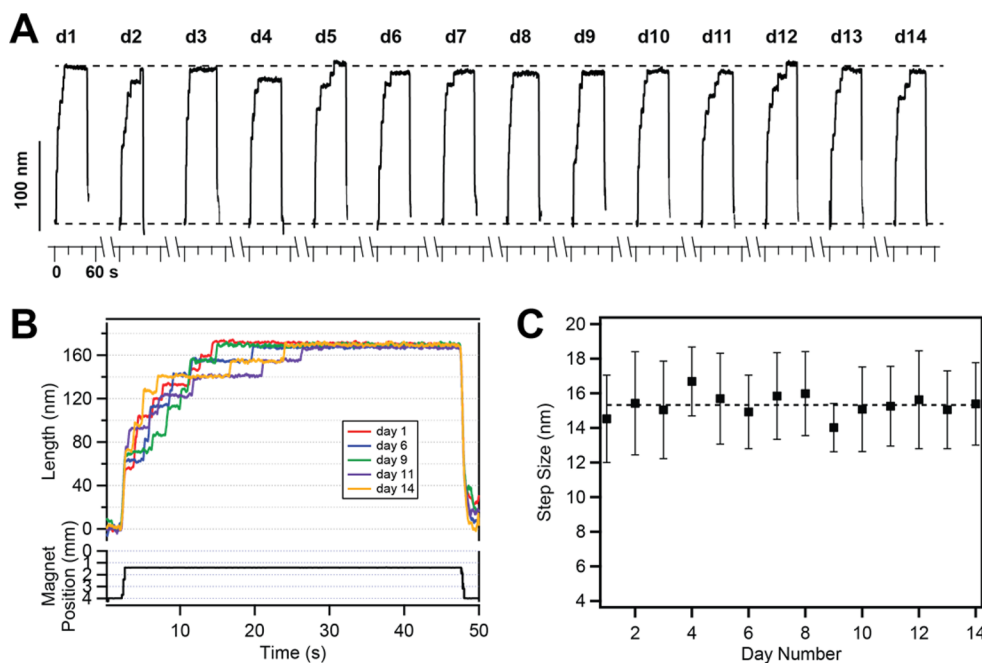


Figure 5. Two-week-long recording of a single HaloTag anchored protein L construct. (A) Daily unfolding pulses to 45 pN (MP = 1.4 mm) track the unfolding kinetics of the same single HaloTag-(protein L)₈-AviTag molecule over 14 days. The molecule was allowed to rest throughout the day in the folded state (4.3 pN; MP = 4.0 mm) with the microscope lights turned off, and was tested daily in the evening (~5 pm). (B) Superimposed traces from (A) showing the full unfolding of the protein L construct at day 1 (red), day 6 (blue), day 9 (green), day 11 (magenta), and day 14 (gold). The unfolding rate stayed similar throughout. (C) Average step sizes per day measured from the unfolding staircases (15.3 ± 0.7 nm). The step sizes remained constant throughout the 2 weeks.

measured each day gave 15.3 ± 0.7 nm, which is within the error of the predicted 14.7 nm calculated from the WLC model for a MP = 1.4 mm (eq 2); the average step sizes betrayed no directional drift (Figure 5C). We can thus conclude that our magnetic tweezers setup and magnet law are suitable for reliable long-term force measurements.

To resolve individually addressable HaloTag-protein L molecules, we modified the magnetic tweezers microscope stage with an *xy*-positioning stage with 100 nm resolution, and developed HaloTag-Ligand-functionalized fluid chambers having a $50 \mu\text{m}^2$ grid array (Figure S2). Using this combination, we could reliably return to individual beads on successive days. The molecule shown in Figure 5 was the longest lasting before detachment (14 days), from an initial group of 17 molecules that were tracked simultaneously and that lasted more than 1 day (7 molecules, 1 day; 3, 2 days; 1, 3 days; 1, 4 days; 1, 5 days; 1, 6 days; 1, 9 days; 1, 10 days; 1, 14 days). It is likely that the loss of anchoring occurred at the noncovalent streptavidin–biotin interface with the paramagnetic bead rather than the HaloTag-chloroalkane interface with the glass surface, which is covalent. Replacing the biotin–streptavidin interface with an orthogonal covalent HaloTag will solve this problem, allowing, in principle, for protein L constructs to be probed indefinitely.

Another potential source of error in the use of our magnet law results from bead-to-bead variations. However, our measurements indicate that for a given magnet position, M-270 paramagnetic beads generate a reproducible force. This is demonstrated in Figure 3D, where the overstretching B–S transition (65 pN) measured for 34 different traces from four different experiments, occurs over a very narrow distribution of magnet positions (MP = 0.99 ± 0.05 mm). Undoubtedly, it is important here to be able to position the magnets in a reproducible manner so that any variation results solely from

the beads themselves. The voice-coil design with the submicron encoder solves this problem by giving a reliable positioning of the magnets between different experiments. Hence, we conclude that there is little variation in force among M-270 beads. Figure S7 compares our data and magnet law, with magnet laws obtained by others using thermal fluctuations of micrometer-long DNA tethers and the same paramagnetic beads (M-270; Dynabeads). It is clear that there is remarkably good agreement between these different methods at forces below 65 pN.^{6c,14} While the change in force with magnet position has been shown to follow a single exponential,²⁰ several studies have proposed that a double exponential magnet law might be needed at higher forces.^{13e,14}

Magnetic tweezers, combined with HaloTag anchoring techniques, are opening up exciting possibilities to study protein dynamics with remarkable stability and accuracy under force clamp conditions. The methods demonstrated in this paper provide a robust approach to estimate the force applied to a protein in the biologically relevant low-force regime of 0–60 pN and for extended periods of time, comparable to protein turnover. These techniques complement force-clamp AFM spectroscopy that excels in speed and resolution at higher forces, but remains limited by mechanical drift in the low-force regime. To our knowledge, the mechanical study of a single protein over a period of 14 days is the longest yet reported. Such long-term recordings allow us to begin to study protein mechanics on the human time scale, where protein folding and misfolding occur over a lifetime, as, for example, with ocular cataracts or chronic traumatic brain injury. This long-term recording was enabled by the HaloTag covalent chemistry used for surface conjugation. Engineering of a second covalent anchor to replace the non-covalent biotin–streptavidin attachment to the magnetic bead would further improve the stability

of the tethers, and could offer the potential for month-long or year-long single-molecule studies where rare events, such as those that take place in vivo, become detectable.

■ ASSOCIATED CONTENT

Supporting Information

The Supporting Information is available free of charge on the ACS Publications website at DOI: 10.1021/jacs.6b05429.

Supplementary materials and methods, including Figures S1–S7 (PDF)

MagneticTweezers_Software (TXT)

■ AUTHOR INFORMATION

Corresponding Authors

*popa@uwm.edu

*jfernandez@columbia.edu

Present Address

†I.P.: Department of Physics, University of Wisconsin–Milwaukee, 3135 N. Maryland Ave., Milwaukee, WI 53211

Notes

The authors declare no competing financial interest.

■ ACKNOWLEDGMENTS

This work was supported by NSF Grant DBI-1252857, and by NIH Grants GM116122 and HL061228. We would like to acknowledge Jie Yan, Hu Chen, and Mingxi Yao from the National University of Singapore for their help with the initial development of the instrument and for sharing the DNA–protein cross-linking protocol. D.J.E. were supported by the MSTP training grant to Columbia University. We thank also to Jaykar Nayeck for contributions to the development of the magnetic tweezers software.

■ REFERENCES

- (1) Schroder, M.; Kaufman, R. J. *Annu. Rev. Biochem.* **2005**, *74*, 739–89.
- (2) (a) Shringarpure, R.; Davies, K. J. *Free Radical Biol. Med.* **2002**, *32*, 1084–9. (b) Hess, D. T.; Matsumoto, A.; Nudelman, R.; Stamler, J. S. *Nat. Cell Biol.* **2001**, *3*, E46–9. (c) Chang, T. C.; Chou, W. Y.; Chang, G. G. *J. Biomed. Sci.* **2000**, *7*, 357–63. (d) Alegre-Cebollada, J.; Kosuri, P.; Giganti, D.; Eckels, E.; Rivas-Pardo, J. A.; Hamdani, N.; Warren, C. M.; Solaro, R. J.; Linke, W. A.; Fernandez, J. M. *Cell* **2014**, *156*, 1235–46.
- (3) Knowles, T. P.; Vendruscolo, M.; Dobson, C. M. *Nat. Rev. Mol. Cell Biol.* **2014**, *15*, 384–96.
- (4) (a) Cao, Y.; Balamurali, M. M.; Sharma, D.; Li, H. *Proc. Natl. Acad. Sci. U. S. A.* **2007**, *104*, 15677–81. (b) Linke, W. A.; Grutzner, A. *Pfluegers Arch.* **2008**, *456*, 101–115.
- (5) Berkovich, R.; Hermans, R. I.; Popa, I.; Stirnemann, G.; Garcia-Manyes, S.; Berne, B. J.; Fernandez, J. M. *Proc. Natl. Acad. Sci. U. S. A.* **2012**, *109*, 14416–14421.
- (6) (a) Janissen, R.; Berghuis, B. A.; Dulin, D.; Wink, M.; van Laar, T.; Dekker, N. H. *Nucleic Acids Res.* **2015**, *42*, e137. (b) Popa, I.; Berkovich, R.; Alegre-Cebollada, J.; Badilla, C. L.; Rivas-Pardo, J. A.; Taniguchi, Y.; Kawakami, M.; Fernandez, J. M. *J. Am. Chem. Soc.* **2013**, *135*, 12762–71. (c) Chen, H.; Yuan, G. H.; Winardhi, R. S.; Yao, M. X.; Popa, I.; Fernandez, J. M.; Yan, J. *J. Am. Chem. Soc.* **2015**, *137*, 3540–3546.
- (7) Liu, R.; Garcia-Manyes, S.; Sarkar, A.; Badilla, C. L.; Fernandez, J. M. *Biophys. J.* **2009**, *96*, 3810–21.
- (8) (a) Fernandez, J. M.; Li, H. B. *Science* **2004**, *303*, 1674–1678. (b) Li, H. B.; Linke, W. A.; Oberhauser, A. F.; Carrion-Vazquez, M.; Kerkvliet, J. G.; Lu, H.; Marszalek, P. E.; Fernandez, J. M. *Nature* **2002**, *418*, 998–1002. (c) Valle-Orero, J.; Eckels, E. C.; Stirnemann, G.;

Popa, I.; Berkovich, R.; Fernandez, J. M. *Biochem. Biophys. Res. Commun.* **2015**, *460*, 434–438.

(9) Brockwell, D. J.; Beddard, G. S.; Paci, E.; West, D. K.; Olmsted, P. D.; Smith, D. A.; Radford, S. E. *Biophys. J.* **2005**, *89*, 506–519.

(10) Garcia-Manyes, S.; Dougan, L.; Badilla, C. L.; Brujic, J.; Fernandez, J. M. *Proc. Natl. Acad. Sci. U. S. A.* **2009**, *106*, 10534–10539.

(11) O'Neill, J. W.; Kim, D. E.; Baker, D.; Zhang, K. Y. J. *Acta Crystallogr., Sect. D: Biol. Crystallogr.* **2001**, *57*, 480–487.

(12) Kosuri, P.; Alegre-Cebollada, J.; Feng, J.; Kaplan, A.; Ingles-Prieto, A.; Badilla, C. L.; Stockwell, B. R.; Sanchez-Ruiz, J. M.; Holmgren, A.; Fernandez, J. M. *Cell* **2012**, *151*, 794–806.

(13) (a) Gosse, C.; Croquette, V. *Biophys. J.* **2002**, *82*, 3314–3329. (b) Charvin, G.; Vologodskii, A.; Bensimon, D.; Croquette, V. *Biophys. J.* **2005**, *88*, 4124–4136. (c) Koster, D. A.; Palle, K.; Bot, E. S. M.; Bjornsti, M. A.; Dekker, N. H. *Nature* **2007**, *448*, 213–217. (d) Lipfert, J.; Kerssemakers, J. W. J.; Jager, T.; Dekker, N. H. *Nat. Methods* **2010**, *7*, 977–U54. (e) Chen, H.; Fu, H. X.; Zhu, X. Y.; Cong, P. W.; Nakamura, F.; Yan, J. *Biophys. J.* **2011**, *100*, 517–523. (f) Zhang, X. H.; Chen, H.; Le, S. M.; Rouzina, I.; Doyle, P. S.; Yan, J. *Proc. Natl. Acad. Sci. U. S. A.* **2013**, *110*, 3865–3870.

(14) Yu, Z.; Dulin, D.; Cnossen, J.; Köber, M.; van Oene, M. M.; Ordu, O.; Berghuis, B. A.; Hensgens, T.; Lipfert, J.; Dekker, N. H. *Rev. Sci. Instrum.* **2014**, *85*, 123114.

(15) (a) Rief, M.; Gautel, M.; Oesterhelt, F.; Fernandez, J. M.; Gaub, H. E. *Science* **1997**, *276*, 1109–1112. (b) Keller Mayer, M. S. Z.; Smith, S. B.; Granzier, H. L.; Bustamante, C. *Science* **1997**, *276*, 1112–1116. (c) Tskhovrebova, L.; Trinick, J.; Sleep, J. A.; Simmons, R. M. *Nature* **1997**, *387*, 308–312. (d) Rivas-Pardo, J. A.; Eckels, E. C.; Popa, I.; Kosuri, P.; Linke, W. A.; Fernandez, J. M. *Cell Rep.* **2016**, *14*, 1339–1347.

(16) (a) Smith, S. B.; Cui, Y.; Bustamante, C. *Science* **1996**, *271*, 795–9. (b) Bianco, P.; Bongini, L.; Melli, L.; Dolfi, M.; Lombardi, V. *Biophys. J.* **2011**, *101*, 866–874.

(17) Popa, I.; Kosuri, P.; Alegre-Cebollada, J.; Garcia-Manyes, S.; Fernandez, J. M. *Nat. Protoc.* **2013**, *8*, 1261–1276.

(18) Carrion-Vazquez, M.; Oberhauser, A. F.; Fowler, S. B.; Marszalek, P. E.; Broedel, S. E.; Clarke, J.; Fernandez, J. M. *Proc. Natl. Acad. Sci. U. S. A.* **1999**, *96*, 3694–3699.

(19) Popa, I.; Fernandez, J. M.; Garcia-Manyes, S. *J. Biol. Chem.* **2011**, *286*, 31072–31079.

(20) (a) Kruithof, M.; Chien, F.; de Jager, M.; van Noort, J. *Biophys. J.* **2008**, *94*, 2343–2348. (b) Lipfert, J.; Hao, X.; Dekker, N. H. *Biophys. J.* **2009**, *96*, 5040–9. (c) De Vlaminck, I.; Henighan, T.; van Loenhout, M. T. J.; Burnham, D. R.; Dekker, C. *PLoS One* **2012**, *7*, e41432.